

Supporting Information

Promising catalytic activity by non-thermal plasma synthesized SBA-15 supported metal catalysts in one-step plasma-catalytic methane conversion to value-added fuels

Piu Chawdhury,^a KVSS Bhargavi,^a M. Selvaraj^b and Ch. Subrahmanyam^{*a}

^a *Department of Chemistry, Indian Institute of Technology Hyderabad, Telangana 502 285, India*

^b *Department of Chemistry, Faculty of Sciences, King Khalid University, Kingdom of Saudi Arabia*

Email: csubbu@iith.ac.in

Contents

1. GC analysis and formula of standard concentration curves.
2. Standard formulas to calculate the conversion of reactant, yields (Y) and selectivity of the gaseous products (S) and liquid oxygenates (S_i).
3. Table S2. Acidic sites of the catalysts from NH₃ TPD.
4. Table S3. Basic sites of the catalysts from CO₂ TPD.
5. The XRD profile of SBA-15.
6. Morphology analysis of SBA-15 support.
7. FESEM images of P-Ag/SBA-15 catalyst.
8. Particle size distribution curves.
9. Color change of the catalysts before and after plasma reduction process.
10. Lissajous figures.
11. Calculation of discharge parameters
12. Optical emission spectroscopy study.
13. The yield plot of the products.
14. Spent catalyst characterization.

15. Table of comparison.

16. References.

1. GC analysis and formula of standard concentration curves.

GC analysis:

The gaseous products were analyzed by an online gas chromatograph (SHIMADZU GC-2014) equipped with a packed column (Hayasep A, 80/100 mesh, 3 m) and a TCD detector. The column temperature and the GC injector temperature were set to 333 K and 413 K, respectively, whereas Ar was used as a carrier gas with the constant flow rate of 5 mL/min. Prior to the reactions, GC/TCD was calibrated using a variety of gases (i.e., CH₄, C₂H₆, CO₂, H₂ and CO) manipulated by a set of mass flow controllers. The condensed liquid products were collected in an ice-cold trap placed at the exit of DBD reactor which were then qualitatively analyzed using a gas chromatography – mass spectrometer (GC-MS, Thermo scientific Trace GC Ultra) and quantitatively analyzed using a gas chromatograph (Thermo scientific Trace GC Ultra) equipped with a FID and a DB-WAX column (length/30 m; diameter/0.25 mm). The injector temperature was set to 513 K followed by a ramp in column temperature (starting from 343 K to 473 K). He was used as a carrier gas with the constant flow rate of 1.2 mL/min. To evaluate the reaction outcomes, the concentration of the liquid products in the condensate was calculated via corresponding formula of standard calibrated concentration curve (Table S1).

Table S1. Formula of standard concentration curves.

Sample	Equation	Adj. R square
Methanol	$y = 1.37235E-7 \times x - 0.0005599$	0.99981
Ethanol	$y = 6.58505E-8 \times x - 0.01202$	0.99898
Acetic acid	$y = 1.09359E-7 \times x + 0.01624$	0.99993
Acetone	$y = 4.78846E-8 \times x - 0.00307$	0.99871
Formaldehyde	$y = 2.06717E-5 \times x + 0.08029$	0.99855
Formic acid	$y = 1.47165E-5 \times x - 0.02457$	0.99967

2. The standard formulas to calculate the conversion of reactant, yields (Y) and selectivity of the gaseous products (S) and liquid oxygenates (S_i):

$$CH_4 \text{ conversion (\%)} = \frac{\text{No. of moles of } CH_4 \text{ converted}}{\text{No. of moles of } CH_4 \text{ input}} \times 100 \quad (S1)$$

$$\text{Selectivity of } CO_x(\%) = \frac{\text{No. of moles of } CO_x \text{ produced}}{\text{No. of moles of } CH_4 \text{ converted}} \times 100 \quad (S2)$$

$$\text{Selectivity of } C_2H_6(\%) = \frac{2 \times \text{No. of moles of } C_2H_6 \text{ produced}}{\text{No. of moles of } CH_4 \text{ converted}} \times 100 \quad (S3)$$

$$\text{Selectivity of } H_2(\%) = \frac{\text{No. of moles of } H_2 \text{ produced}}{2 \times \text{No. of moles of } CH_4 \text{ converted}} \times 100 \quad (S4)$$

The selectivity of the liquid products can be calculated as:

$$\text{Total liquid oxygenates selectivity (\%)} = 100 - (S_{CO} + S_{CO_2} + S_{C_2H_6}) \quad (S5)$$

$$S_i(\%) = \frac{n_i C_i}{\sum n_i C_i} \times eq (5)$$

n_i = Carbon number in the liquid oxygenate, i

C_i = moles of Carbon containing liquid oxygenate

$$\text{Yield of products (\%)} = \text{Selectivity} \times CH_4 \text{ conversion (\%)} \quad (S7)$$

$$\begin{aligned} &\text{Energy efficiency for } CH_4 \text{ conversion (mmol/kJ)} \\ &= \frac{CH_4 \text{ converted (mmol/min)}}{\text{Discharge power (W)}} \times \frac{1000}{60} \end{aligned} \quad (S8)$$

3. Table S2. Acidic sites of the catalysts from NH₃ TPD.

Sample	Weak acidic site (mmol/g)	Strong acidic site (mmol/g)	Total acidic site (mmol/g)
SBA-15	0.01	0.018	0.028
P-Pd/ SBA-15	0.008	0.023	0.031

P-Pt/ SBA-15	0.008	0.027	0.035
P-Ag/ SBA-15	0.005	0.017	0.022
P-Au/ SBA-15	0.005	0.020	0.025

4. Table S3. Basic sites of the catalysts from CO₂ TPD.

Sample	Weak basic site (mmol/g)	Strong basic site (mmol/g)	Total basic site (mmol/g)
SBA-15	0.006	0.258	0.264
P-Pd/ SBA-15	0.008	0.497	0.505
P-Pt/ SBA-15	0.008	0.405	0.413
P-Ag/ SBA-15	0.005	0.509	0.514
P-Au/ SBA-15	0.005	0.377	0.382

5. The XRD profile of SBA-15 has been also recorded and presented below.

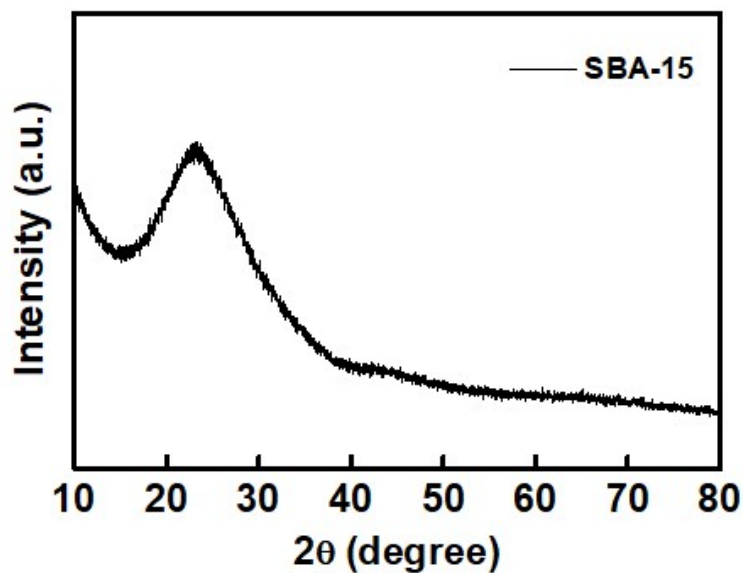


Fig. S1. XRD profile of only SBA-15.

6. Morphology analysis of SBA-15 support.

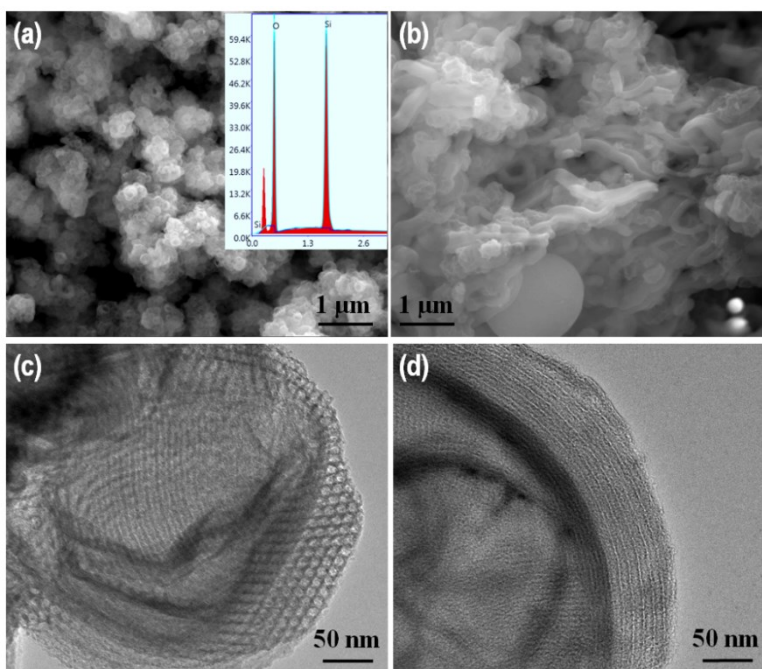


Fig. S2. (a), (b) FESEM images of SBA-15 with EDS mapping. (c), (d) TEM images of SBA-15.

7. High resolution FESEM images of P-Ag/SBA-15 catalyst shows that some Ag nanoparticles are reflecting above the support surface which means some of them are not confined properly in the pore channels of SBA-15.

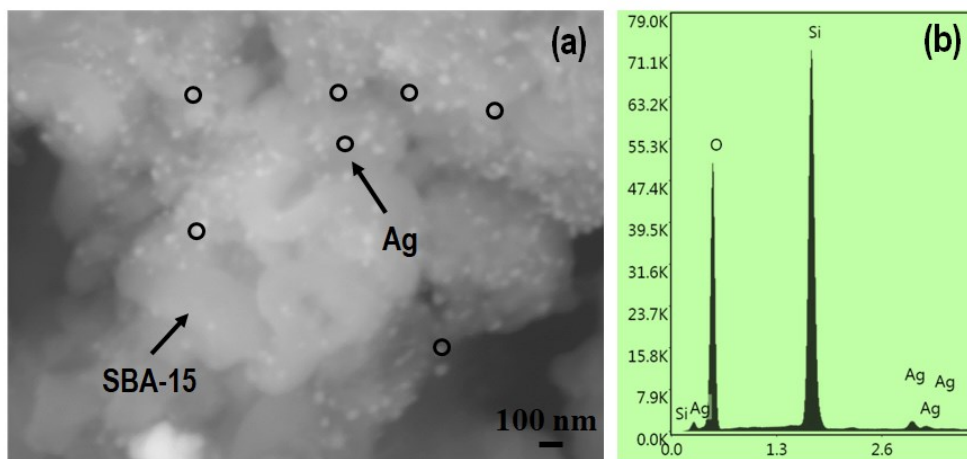


Fig. S3. High magnification FESEM images of SBA-15 with corresponding EDS mapping. Particle size distribution curves are derived from several TEM images of the following samples and presented below.

8. Particle size distribution curves.

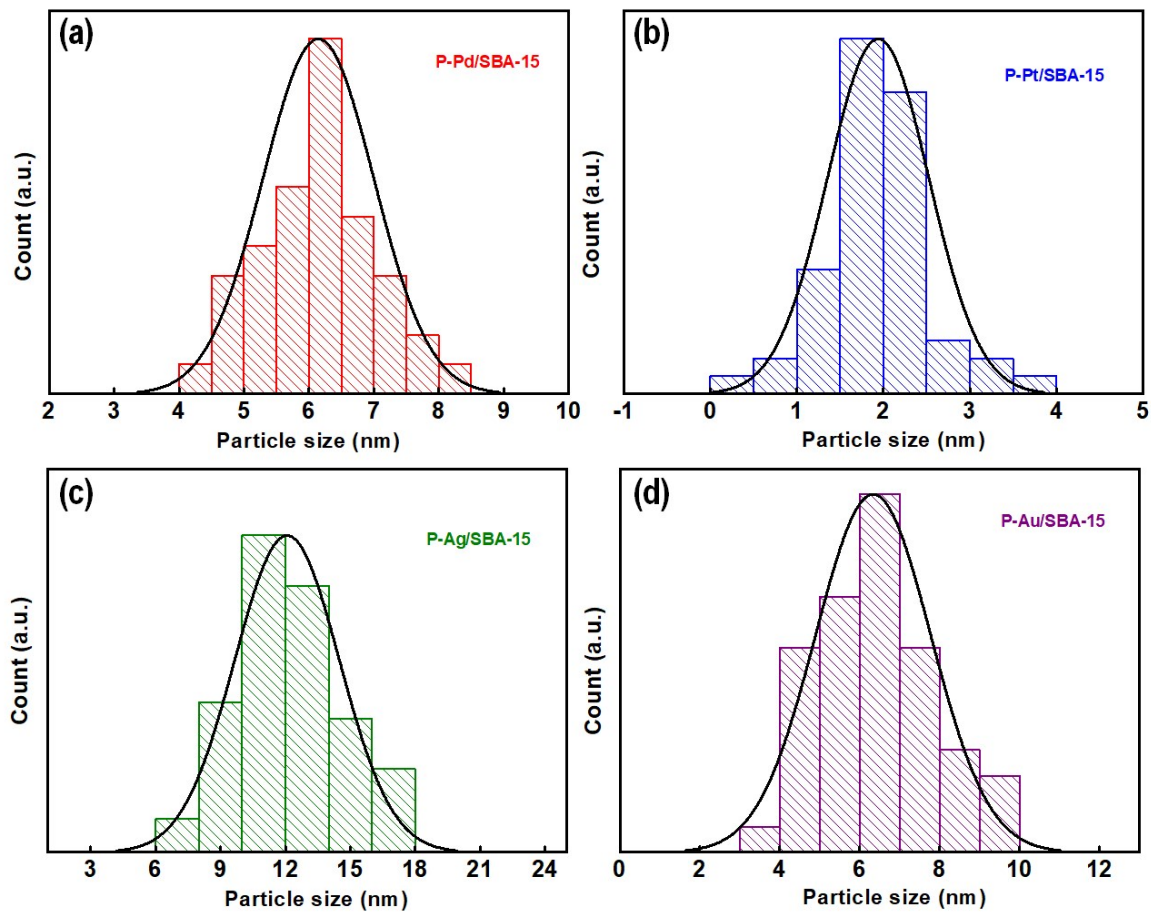


Fig. S4. Particle size distribution curves for (a) P-Pd/SBA-15 (b) P-Pt/SBA-15 (c) P-Ag/SBA-15 and (d) P-Au/SBA-15 catalysts.

9. Color change of the catalysts before and after plasma reduction process.

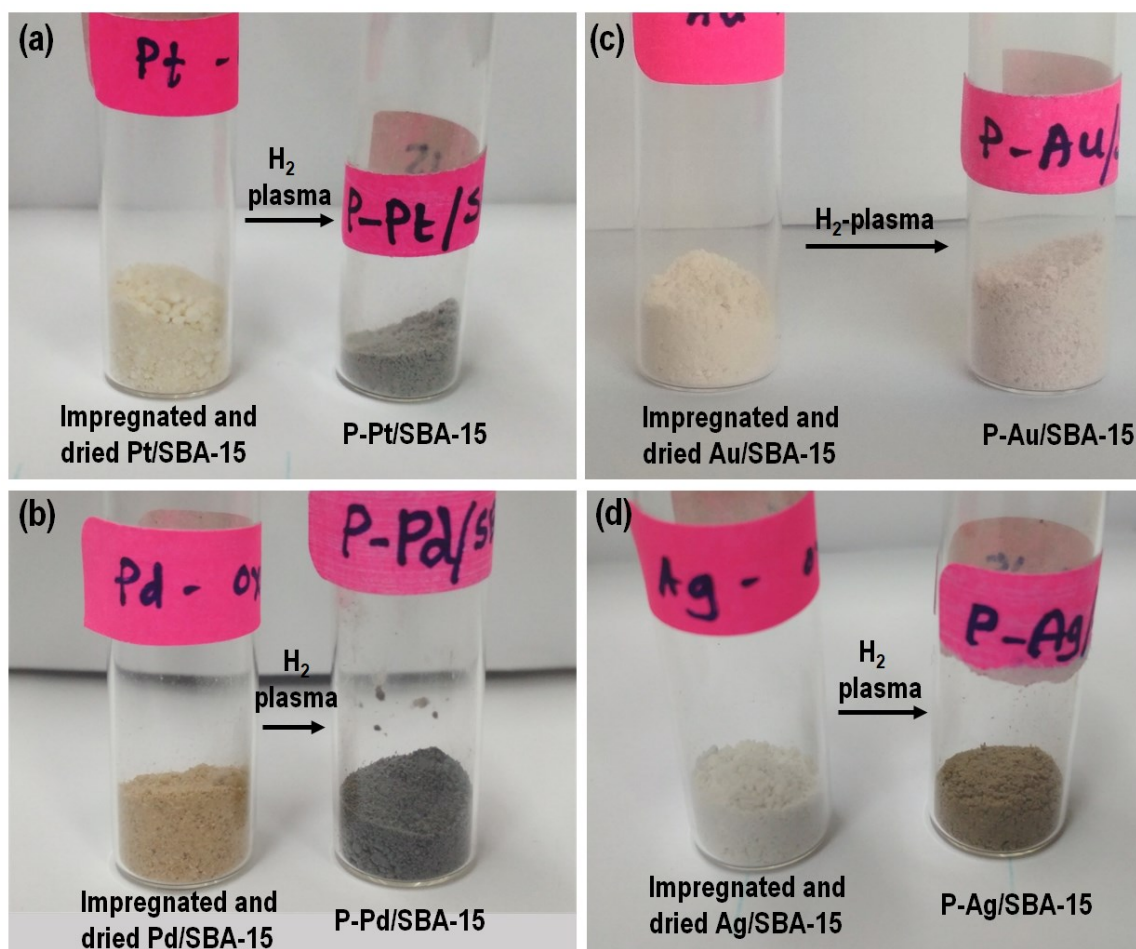


Fig. S5. As synthesized catalysts before and after plasma treatment. (a) Pt/SBA-15 (b) Pd/SBA-15 (c) Au/SBA-15 and (d) Ag/SBA-15.

10. The power applied for the plasma reduction process was calculated from the following Lissajous figure.

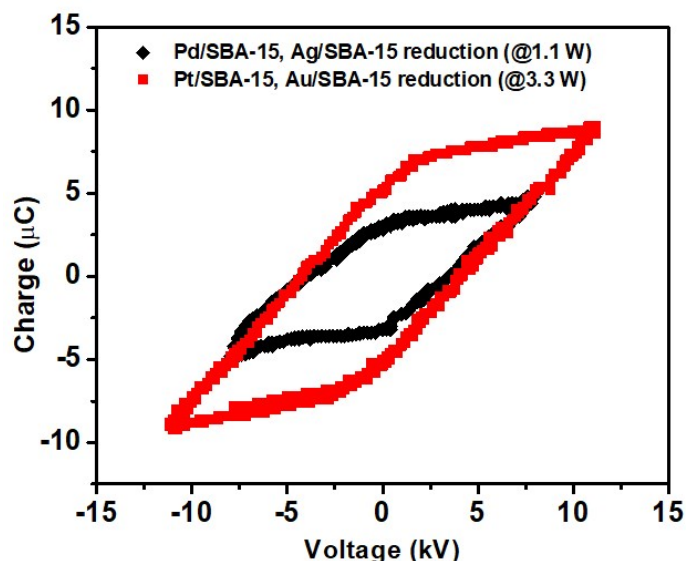


Fig. S6. Lissajous figures for plasma-reduction process.

11. Calculation of discharge parameters

The discharge parameters have been calculated from the Lissajous figures recorded for both only NTP and PC-NTP systems. Here, a schematic diagram of Lissajous figure is presented to describe the details. Fig. S6a represents the equivalent circuit of the NTP-DBD reactor, which consists of two capacitors in a series connection. One is the C_g , the capacitance of the gas gap and C_d is the capacitance associated with the dielectric barrier. When the discharge is active, the apparent capacitance of the DBD reactor is equal to the capacitance of dielectric barrier alone (C_d); but in presence of inactive discharge, the reactor capacitance is equal to the series combination of C_d and C_g . In the presence of the solid catalyst in the gas gap, C_g represents the contribution of the gas–solid integration in the inter-electrode region and C_d is considered to be equal with the effective capacitance (C_{eff}) when the discharge zone is fully packed. Fig. S6b presents the corresponding schematic diagram of Q-V Lissajous figure where, lines AB and CD represent the discharge-on phase (active) when gas break-down occurs with plasma ignition. The slope of these lines is the

effective capacitance (C_{eff}). Lines BC and DA represent the discharge-off phase when there only displacement current is present. The slope of the lines BC and DA corresponds to C_{cell} in the plasma-off period (inactive), which is formed by the dielectric capacitance C_d and the capacitance of the gap C_g .

$$\frac{1}{C_{\text{cell}}} = \frac{1}{C_d} + \frac{1}{C_g}$$

The breakdown voltage can be calculated as

$$V_b = \frac{1}{1 + (C_g/C_d)} \times V_{\text{min}}$$

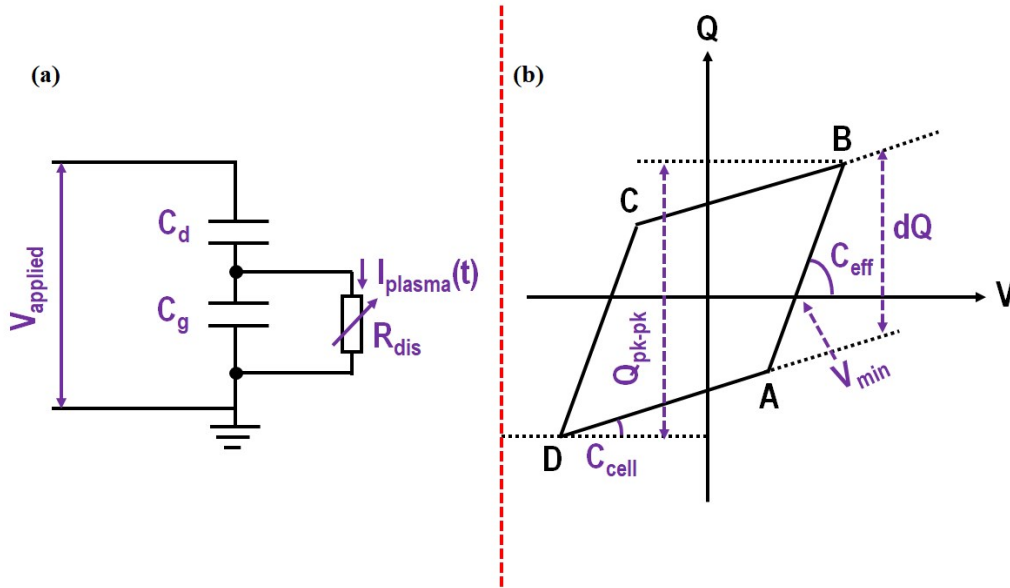


Fig. S7. (a) Equivalent circuit for the DBD and (b) the corresponding Q-V Lissajous diagram.

12. Optical emission spectroscopy study

The optical emission spectroscopy technique was performed to identify the active species generated inside the plasma discharge reactor during the partial oxidation of methane. Generally, in non-equilibrium plasma the chemical reactions are initiated with the fast electron ionization process followed by the formation of several active species like CH, CO, O, H, C_2 , H_2 , CO_2 etc as seen in Fig. S8. The characteristic peaks of CH at 431 nm and 317 nm along with the O active

species appeared at 777.7 nm support the decomposition of the reactant gases, while CO₂ (391 nm) and CO Angstrom band (450–561 nm) directly confirms the products formation.

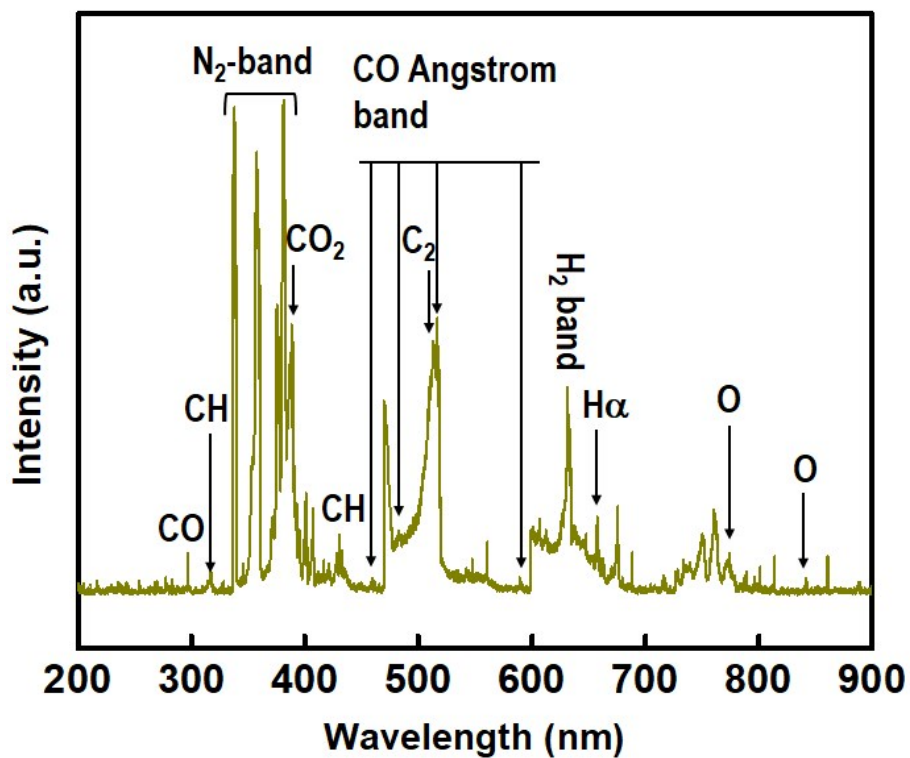


Fig. S8. OES spectra of CH₄ and O₂ combined plasma system. (CH₄:O₂ = 5:1; Total flow rate = 30 mL/min; Power = 1.7 W; Frequency = 50 Hz).

13. The yield of the products was calculated from Eq. S7.

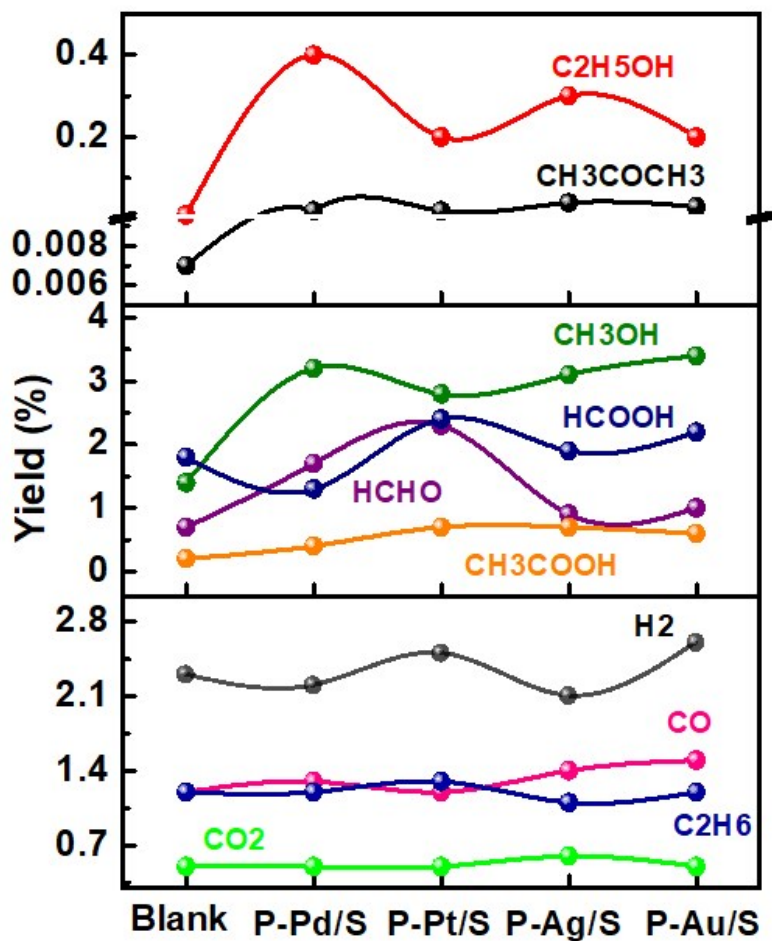


Fig. S9. Distribution curve of product yields ($\text{CH}_4:\text{O}_2 = 5:1$; Total flow rate = 30 mL/min; Power = 1.7 W; Frequency = 50 Hz).

14. Spent catalyst characterization

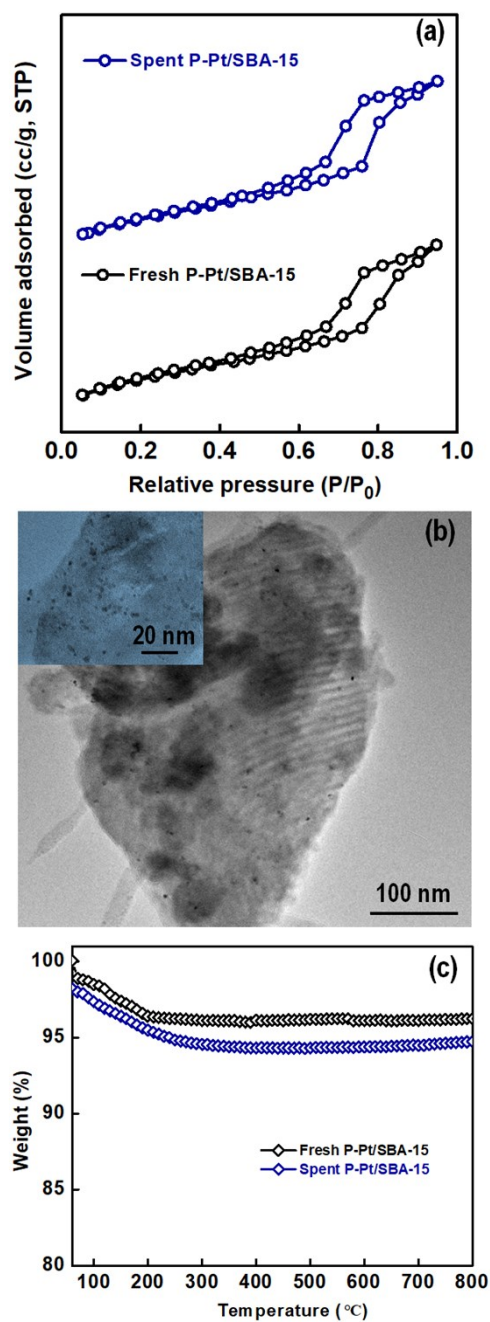


Fig. S10. Spent P-Pt/SBA-15 catalyst characterization (a) N₂ adsorption-desorption isotherm (b) TEM images (c) TGA profile.

15. Table of comparison

Table S4: Comparative data from several literatures.

Reactor system	Catalyst	Reactants	Power (W)	CH ₄ conversion (%)	CH ₃ OH Selectivity (%)	Total liquid selectivity (%)	Reference
DBD	Ga/CZA	CH ₄ , O ₂	50	54.5	22.2	-	[1]
DBD	Ni/YSZ	CH ₄ , O ₂ He	80	35.3	23.5	-	[2]
DBD	He-O ₂ -H ₂ plasma treated Fe/Hf/YSZ	CH ₄ , O ₂ , He	80	35	28.5	-	[3]
DBD	Cu-Zn-Al	CH ₄ , O ₂ , He	60-80	25.3	23	-	[4]
DBD + Temp	Fe ₂ O ₃ /CP	CH ₄ , Air	140	25.5	10.5	-	[5]
DBD + Temp	Fe ₂ O ₃ /Cu O/CP	CH ₄ , Air	140	25	11.2	-	[6]
DBD + Temp	Fe ₂ O ₃ /Cu O/ γ - Al ₂ O ₃	CH ₄ , Air	120	43	3.7	-	[7]
DBD	Cu- Ni/CeO ₂	CH ₄ , N ₂ O	6	23	36	49	[8]
DBD	Cu/ γ - Al ₂ O ₃	CH ₄ , O ₂	1.9	9	37	66	[9]
DBD	Cu/ZnO/	CH ₄ , Air	1.7	10	25	50	[10]

	γ -Al ₂ O ₃						
DBD	Pt/ γ -Al ₂ O ₃	CH ₄ ,CO ₂	10	17	10	6	[11]
DBD	Fe/SiO ₂	CH ₄ ,CO ₂	9.5	47	31	48	[12]
DBD	P-Pd/SBA-15	CH ₄ , O ₂	1.7	10	32	70	This work

16. References

1. A. Indarto. *Ionics*, 2014, **20**, 445-449.
2. A. Indarto, H. Lee, J.W. Choi and H.K. Song, *Energy Sources, Part A*, 2008, **30**, 1628–1636.
3. A. Indarto, J.W. Cho, H. Lee, H.K. Song and J. Palgunadi, *J. Rare Earths*, 2006, **24**, 513-518.
4. A. Indarto, D.R. Yang, J. Palgunadi, J.W. Choi, H. Lee and H.K. Song, *Chem. Eng. Process.*, 2008, **47**, 780-786.
5. L. Chen, X.W. Zhang, L. Huang and L.C. Lei, *Chem. Eng. Process.*, 2009, **48**, 1333-1340.
6. L. Chen, X. Zhang, L. Huang and L. Lei, *Chem. Eng. Technol.*, 2010, **33**, 2073-2081.
7. L. Chen, X. Zhang, L. Huang and L. Lei, *J. Nat. Gas. Chem*, 2010, **19**, 628-637.
8. S. Mahammadunnisa, K. Krushnamurthy and C. Subrahmanyam, *Catal. Today*, 2015, **256**, 102-107.
9. P. Chawdhury, D. Ray, T. Vinodkumar and C. Subrahmanyam, *Catal. Today*, 2019, **337**, 117-125.
10. P. Chawdhury, D. Kumar and C. Subrahmanyam, *Chem. Eng. J.*, 2019, **372**, 638-647.
11. L. Wang, Y. Yi, C. Wu, H. Guo, X. Tu, *Angew. Chem. Int. Ed.*, **2017**, 56, 13679-13683.
12. D. Li, V. Rohani, F. Fabry, A. P. Ramaswamy, M. Sennour and L. Fulcheri, *App. Catal. B: Environ.*, 2020, **261**, 118228.